European Polymer Journal 201 (2023) 112531

Contents lists available at ScienceDirect

European Polymer Journal

journal homepage: www.elsevier.com/locate/europolj

Polybenzoxazines as new photothermal therapy agents

Kevin Reyes-Mateo [a], Oriol Careta [b], Jordi Hernando [a,*], Carme Nogués [b,*], Rosa María Sebastián [a,*]

[a] Departament de Química and Centro de Innovación en Química Avanzada (ORFEO-CINQA), Universitat Autònoma de Barcelona, 08193 Cerdanyola del Vallès, Spain
[b] Departament de Biologia Cel.lular, Fisiologia i Immunologia, Universitat Autònoma de Barcelona, 08193 Cerdanyola del Vallès, Spain

ARTICLE INFO

Keywords:
Polybenzoxazine
Photothermal therapy
Nanoparticles
Phototoxicity
Cancer treatment

ABSTRACT

To make photothermal therapy an attractive alternative to conventional cancer treatments, the development of novel photothermal agents with enhanced properties is demanded. To tackle this challenge, herein we explored the use of polybenzoxazines, a well-known class of phenolic resins. Two different types of polybenzoxazine materials were prepared as potential photothermal agents: water-soluble polybenzoxazines as well as nanoparticles of hydrophobic polybenzoxazines, which can be generated in situ by polymer addition to cell culture medium. For both systems, irradiation with visible light led to significant photothermal effects, whose application to photoinduce human breast cancer cell's death was investigated in vitro. The best results were obtained for polybenzoxazine nanostructures, which exhibited successful cell internalization, minimal cytotoxicity in the dark and efficient photothermal killing of cancer cells upon illumination with high-penetrating red light. In combination with their low cost and facile preparation, this makes these polymer nanomaterials highly promising for photothermal therapy applications.

1. Introduction

Photothermal therapy (PTT) has emerged as a highly promising strategy for cancer treatment, which seeks to induce selective cell death in tumors through the heat caused upon local irradiation [1,2–3]. As a result, it allows tumors to be ablated (or inhibited) with spatio-temporal precision while minimizing side effects on healthy tissues. Although this effect can be accomplished directly under high intensity illumination [2], PTT generally makes use of photothermal agents to locally generate heat after light absorption at milder photoexcitation conditions [4–5,6]. To maximize the therapeutic efficacy, several features are demanded for these materials to be used in PTT [4–6]: strong absorption in the spectral regions where biological tissues are more transparent, thus enabling higher penetration depths (e.g., in the therapeutic NIR-I window ranging from 650 nm to 950 nm); efficient conversion of absorbed photons into thermal heat; low toxicity in the dark; high affinity for tumor cells; simple and low-cost fabrication; and even additional theranostic properties (e.g., treatment imaging [7,8] or simultaneous release of a drug for synergic therapeutic effects [9,10]).

To date a variety of photothermal agents have been explored for PTT [4–6]. On the one hand, inorganic materials [11] such as plasmonic metal nanostructures [12,13], carbon-based nanomaterials [14,15] and semiconductor nanoparticles [16] have been thoroughly investigated, especially due to their large absorption in the therapeutic NIR regions and strong photothermal effects. However, they typically suffer from high cost, complex synthesis, non-biodegradability and/or long-term toxicity. Alternatively, the development of organic PTT materials has been proposed [17], which are primarily made of conjugated polymers [18,19] and small dye molecules [20,21]. Unfortunately, they also present various limitations. For instance, the range of choice of conjugated polymers with optimal photothermal properties is limited and, because of their hydrophobicity, they often require previous nanostructuration and surface functionalization to become water-dispersible. As for small dye molecules, they must be normally anchored or loaded into adequate vehicles (e.g., liposomes, peptides) for injection into biological tissues. Accordingly, the development of novel organic PTT agents is required to overcome these drawbacks.

To reach this goal, herein we pioneered the utilization of polybenzoxazines (PBz), a well-known class of high-performance phenolic resins, as PTT materials [22,23]. While PBz have drawn the attention of industry due to their superior thermal, mechanical and chemical properties over traditional thermosets [24–28], their applications in biology and medicine are still limited and essentially related to their use as scaffold [29–30] and antimicrobial [31–34] materials. Recently, when

* Corresponding authors.
E-mail addresses: jordi.hernando@uab.cat (J. Hernando), carme.nogues@uab.cat (C. Nogués), rosamaria.sebastian@uab.cat (R.M. Sebastián).

https://doi.org/10.1016/j.eurpolymj.2023.112531
Received 29 July 2023; Received in revised form 5 October 2023; Accepted 21 October 2023
Available online 28 October 2023

investigating the photothermal polymerization of benzoxazines in the presence of metal catalysts [35], we found that the resulting PBz can also efficiently generate photothermal heat upon visible light absorption, a very intriguing behavior that to the best of our knowledge has not been previously disclosed. In this work we exploited this feature, together with the low cost, simple preparation and ample chemical tunability of polybenzoxazines, to produce a new generation of organic PTT agents.

2. Results and discussion

2.1. Synthesis and nanostructuration of polybenzoxazines

To widely explore the application of polybenzoxazines as PTT materials, we considered two limit scenarios: (a) the fabrication of nanoparticles of water-insoluble PBz that could be dispersed in aqueous media and behave as PTT nanomaterials; and (b) the preparation of water-soluble PBz which could be directly injected into biological tissues without prior structuration and, therefore, act as molecular photothermal agents (Fig. 1a). For this purpose, 1,3-benzoxazine monomers **Bz1** [36] and **Bz2** [37] were first synthesized using reported procedures (Fig. 1b and Scheme S1). **Bz1** bearing a *p*-methoxy substituent was selected as the precursor of water-insoluble PBz because of its efficient synthesis, facile manipulation and strong photothermal effects upon bulk polymerization observed previously by our group [35]. As for **Bz2**, it was selected to favor aqueous solubility for the resulting PBz upon ionization of its *p*-carboxylic acid group.

Both benzoxazine monomers were polymerized thermally at 180–200 °C to yield **PBz1** and **PBz2**, for which neither catalysts nor activators were used that could eventually interfere with our biological measurements (Fig. 1b). Full conversion of the monomers was determined by ^{1}H NMR spectroscopy, which also unambiguously demonstrated the formation of the expected polymer materials (Fig. S1). Further characterization of **PBz1** and **PBz2** by ^{1}H NMR, gel permeation chromatography (GPC), differential scanning calorimetry (DSC) and gel content analysis revealed that they were mainly composed of low molecular weight polymer chains ($M_n \sim 800$ Da) presenting a predominant phenolic structure and negligible chemical cross-linking (Fig. S1-S3 and Scheme S2). As expected [22,23], this resulted in relatively low glass temperatures for these polymer materials ($T_g < 85$ °C) and high solubilities in a large range of organic solvents (e.g., THF, acetone and DMSO). Finally, **PBz2** was treated with an equimolar amount of aqueous NaOH solution to obtain the sodium polybenzoxazine salt **PBz2′** (Fig. 1b). Efficient deprotonation of the carboxylic acid moieties of **PBz2** was confirmed by IR spectroscopy (Fig. S4), which led to high aqueous solubility for the resulting **PBz2′**.

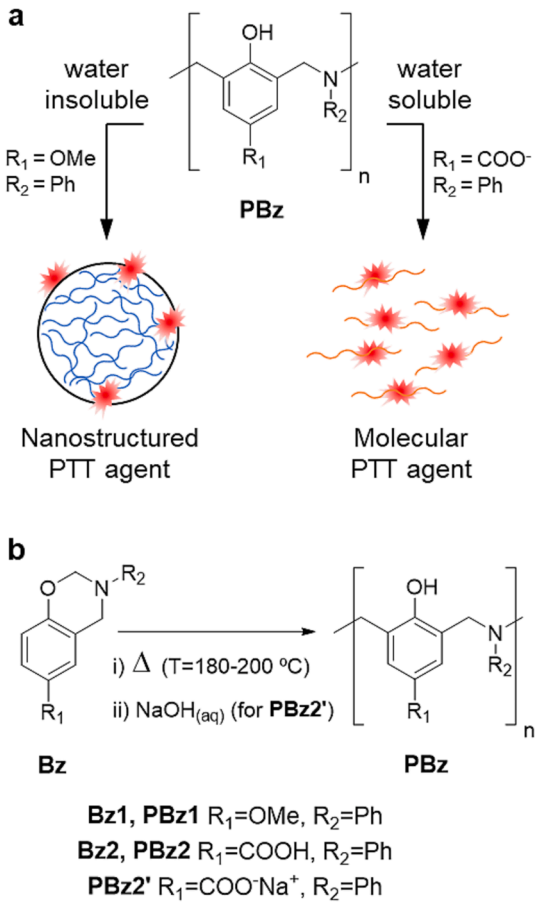

Fig. 1. (a) Water-insoluble and water-soluble polybenzoxazines are explored in this work as nanostructured and molecular photothermal therapy agents, respectively. (b) Synthesis of polybenzoxazines for the preparation of PTT agents.

By contrast, **PBz1** was observed to be insoluble in aqueous media, the reason why it was applied for the preparation of polybenzoxazine nanoparticles (NPs). For this, we first attempted the use of the nanoemulsion technique, a very common approach for the preparation of polymer nanoparticles [38,39]. In particular, we employed an emulsion-solvent evaporation method where (a) a mixture of water and a dichloromethane solution of **PBz1** was initially emulsified through ultrasonication, and (b) the organic solvent was then removed under vacuum to obtain a colloidal aqueous suspension of nanoparticles (**PBz1_NP1**). To favor colloidal stability, this process was conducted in the presence of different well-known stabilizers such as poly(ethylene glycol) 2000, poly(vinyl alcohol) or Tween® 20. Surprisingly, the best results were obtained in the absence of such stabilizers, as the naked **PBz1_NP1** prepared presented the smallest sizes (diameter = 210 ± 37 nm; Fig. 2a and Fig. S5) and were stable in aqueous suspension for 1 week (Fig. S6). The latter can be ascribed to the relatively high ζ-potential of **PBz1_NP1**, which we measured to be + 56.3 mV.

To further simplify the structuration of **PBz1**, we also explored the nanoprecipitation technique [40,41]. In this case, polymer NPs were prepared by just adding a DMSO solution of **PBz1** directly to cell culture medium – i.e., forming in situ the desired nanoparticles in the same medium where biological experiments were subsequently performed. In this way, we avoided prior manipulation, structuration and surface functionalization of **PBz1**, which is a very advantageous feature over most nanostructured PTT agents. In particular, nanoparticles with an average diameter of 78 ± 23 nm were obtained through this procedure, which are significantly smaller than those prepared by the nanoemulsion method (**PBz1_NP2**; Fig. 2b and Fig. S7). However, the colloidal stability of **PBz1_NP2** was found to be much lower, probably due to their low ζ-potential (-7.2 mV). As a result, the formation of aggregates of several hundreds of nanometers in diameter was observed both by scanning electron microscopy (Fig. 2b) and dynamic light scattering measurements (Fig. S8) even for freshly prepared samples.

2.2. Optical and photothermal properties of polybenzoxazines

Fig. 3a shows the absorption spectra of the different photothermal agents developed: (a) the nanostructured **PBz1_NP1** and **PBz1_NP2** in cell culture media, which are compared to the absorption spectrum of **PBz1** dissolved in DMSO; and (b) the aqueous-soluble **PBz2′** in water. Clearly, maximum absorption was observed at $\lambda_{abs} < 450$ nm for all the measured solutions and suspensions. However, long absorption tails were registered for **PBz1_NP1**, **PBz1_NP2** and **PBz2′** that reach up to 700 nm. Therefore, this should allow these polymer materials and molecules to be excited with visible light to trigger their photothermal behavior.

To validate this hypothesis, two different types of photothermal experiments were conducted. First, we took advantage that both **PBz1_NP1** and **PBz2′** could be isolated as solid powders to investigate

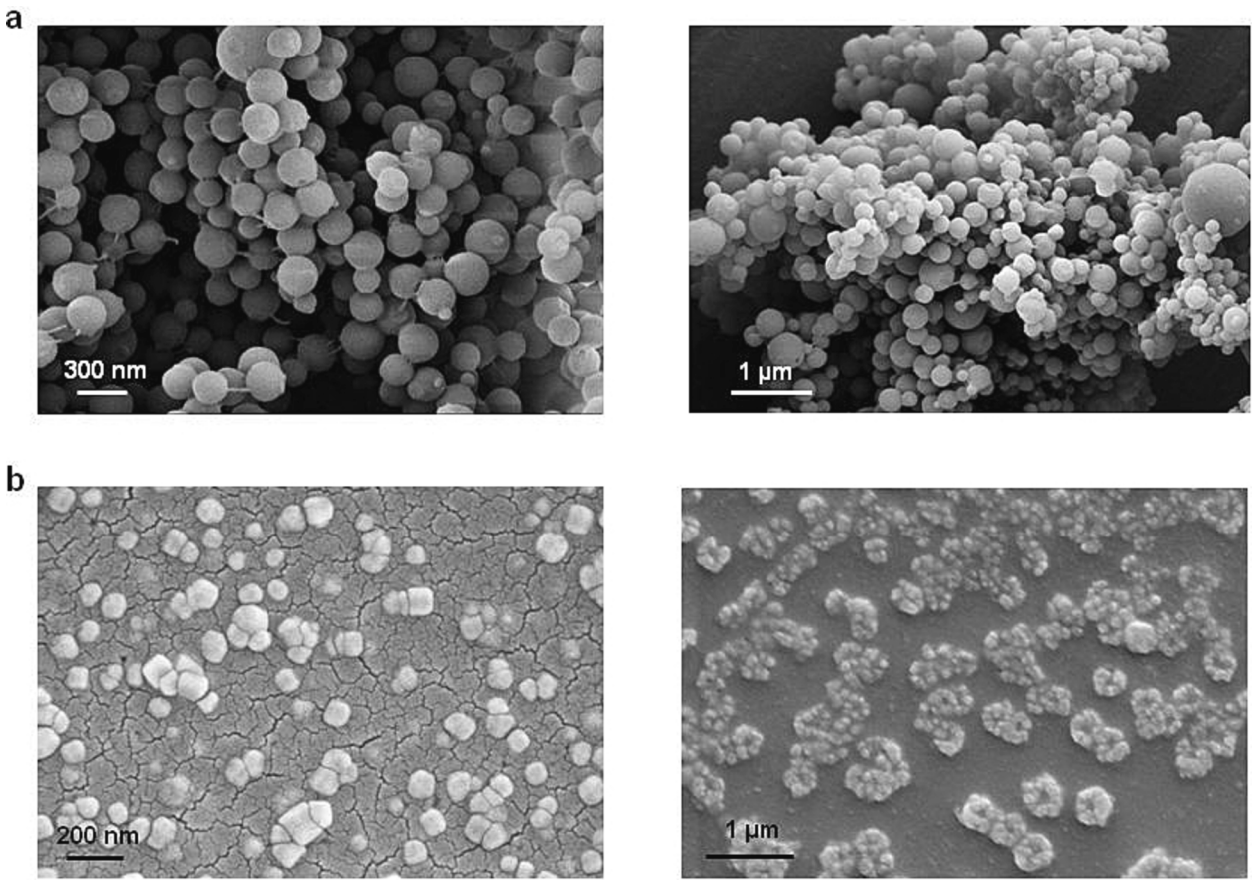

Fig. 2. SEM images of (a) **PBz1_NP1** and (b) **PBz1_NP2**.

their photothermal behavior in bulk. For this, they were irradiated with a pulsed green laser (λ_{exc} = 532 nm, 300 mW cm^{-2}) and the increments in temperature produced by photothermal heating were measured (Fig. S9a). A significant temperature rise of about 8–9 °C was registered in both cases after illumination for 10 min, which demonstrates their capacity to generate heat under irradiation with visible light. In the case of **PBz1_NP2**, its photothermal behavior could only be measured in aqueous suspension. In particular, we monitored the changes in temperature of suspensions of **PBz1_NP1** and **PBz1_NP2** in cell culture medium when irradiated with a white LED (105 mW cm^{-2}). For the polymer concentration used in these experiments (0.43 mg mL^{-1}), temperature increments of around 6 °C were measured in both cases that are clearly higher than those registered in the absence of **PBz1** nanostructures, which again corroborates their photothermal properties upon visible illumination (Fig. 3b). In addition, it must be noted that macroscopic temperature variations averaged over the whole irradiated volume were obtained in these measurements, which must be much smaller than those achieved in the close proximity of **PBz1** nanostructures because of the local nature of photothermal effects. Consequently, we should expect the photothermal heating created by **PBz1** and **PBz2′** be sufficient to induce local cell death. Furthermore, we found these photothermal effects to be reproducible upon consecutive irradiation cycles, thus demonstrating the photostability of the polybenzoxazine materials described herein (Fig. S9b).

2.3. *In vitro photothermal therapy activity of polybenzoxazines*

The PTT activity of **PBz1_NP1**, **PBz1_NP2** and **PBz2′** was tested in vitro on the SKBR-3 human breast cancer cell line. First, we evaluated the intrinsic toxicity of these polybenzoxazine materials in the dark, for which we incubated SKBR-3 with three different concentrations of **PBz1_NP1**, **PBz1_NP2** and **PBz2′** (0.86, 0.43 and 0.22 mg mL^{-1} for **PBz1_NP1** and **PBz1_NP2**; 0.91, 0.46 and 0.23 mg mL^{-1} for **PBz2′**). Slightly different mass concentrations were used for **PBz1_NP1** and **PBz1_NP2** relative to **PBz2′**, with which we aimed to account for the distinct molecular masses of the monomeric units in **PBz1** and **PBz2′**. After 24 h incubation, cell media were gently rinsed to eliminate any uninternalized polymer material and cell viability was evaluated immediately (cell viability 0 h) or after 48 h in standard culture conditions (cell viability 48 h). As shown in Fig. 4a, different degrees of cytotoxicity were detected depending on the tested polybenzoxazine. On the one hand, **PBz1** nanostructures showed very reduced cytoxicity even after 48 h post-incubation for the two lower concentrations tested (0.43 and 0.22 mg mL^{-1}), as cell viabilities remained above 88 % in all the cases. However, for the highest concentration considered (0.86 mg mL^{-1}), cytotoxicity significantly increased, especially for the smaller **PBz1_NP2** nanoparticles (cell viability down to 52 % after 48 h post-incubation). On the other hand, **PBz2′** turned to be more cytotoxic, as an important reduction in cell viability was determined for all conditions except for the lowest concentration and cell culture time (89 % at 0.23 mg mL^{-1} and 0 h post-incubation). In view of these results, we hypothesize that the nanostructuration of polybenzoxazines lowers their cytotoxicity, probably by reducing the contact area with biological tissue per polymer molecule.

Next, the photoinduced cytotoxicity of **PBz1_NP1**, **PBz1_NP2** and **PBz2′** was evaluated. In all the experiments, cell irradiation was conducted with red light (λ_{exc} = 620 – 630 nm, power density = 55 mW cm^{-2}), as it provides higher penetration depths and lower photodamage in biological tissues. In addition, the excitation wavelengths selected fall within the absorbance tail of all the polybenzoxazine materials tested (see Fig. 3a), which should ensure sufficient photoexcitation. It must be noted that, though low light absorption is expected in this spectral

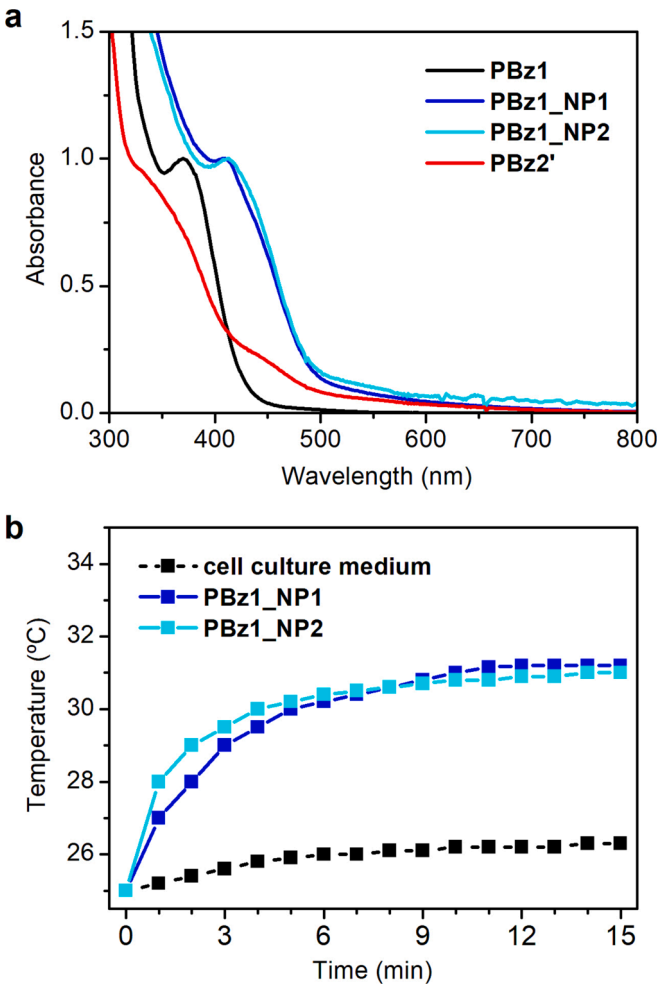

Fig. 3. (a) Absorption spectra of **PBz1** in DMSO ($c = 0.11$ mg mL^{-1}), **PBz1_NP1** and **PBz1_NP2** in cell culture media ($c = 0.11$ mg mL^{-1}) and **PBz2′** in water ($c = 0.13$ mg mL^{-1}). For comparison purposes, all the spectra are normalized to 1.0 at the absorption maximum at $\lambda_{abs} \sim 300 - 450$ nm. (b) Temperature increments measured upon irradiation with a white LED (105 mW cm^{-2}) of 2 mL of pure cell culture medium and 2 mL of **PBz1_NP1** and **PBz1_NP2** suspensions in cell culture media ($c = 0.43$ mg mL^{-1}).

range, we recently demonstrated that Bz monomers and polymers can generate high photothermal effects even under these irradiation conditions [35]. In a first step, we aimed to evaluate the PTT activity of **PBz2′** molecules relative to **PBz1** nanostructures, for which we selected **PBz1_NP2** as the system of study. Because **PBz2′** had shown significant cytotoxicity in the dark, we conducted these comparative studies at low polybenzoxazine concentration (0.22 mg mL^{-1} and 0.23 mg mL^{-1} for **PBz1_NP2** and **PBz2′**), at which SKBR-3 cells were incubated for 24 h. Next, they were irradiated with red light for 30 min to elicit the photothermal response from the internalized polymers and its effect on cell viability was evaluated immediately after irradiation (cell viability 0 h) and 48 h after irradiation (cell viability 48 h) (Fig. 4b). Two main conclusions could be drawn from these experiments. First, phototoxicity was observed even for the control samples containing no **PBz1_NP2** or **PBz2′**, where cell viability decreased down to 78 % after 48 h post-irradiation. Therefore, this demonstrated that irradiation for 30 min at our experimental conditions was excessive for the cells and it should be reduced. In spite of this, the photothermal effects generated by **PBz2′** on cell viability were rather low when compared to the data registered in the absence of illumination: only a reduction of 11 % and 9 % on cell viability was observed under irradiation after 0 h and 48 h, respectively, which fell within the error margins of our data. By contrast, larger phototoxicity was measured for **PBz1_NP2**, with which a statistically significant decrement in cell viability of about 25–30 % was registered relative to equivalent experiments conducted without irradiation.

Because of the higher phototoxicity and lower dark cytotoxicity observed for **PBz1_NP2**, subsequent photothermal experiments were solely conducted for **PBz1** nanostructures. Two important differences were introduced in these additional measurements. On the one hand, higher polybenzoxazine concentrations were used: 0.86 mg mL^{-1} for **PBz1_NP1** and 0.43 for **PBz1_NP2**, which according to our previous cytotoxicity experiments should keep cell viability in the dark over 80 % even after 48 h post-incubation. On the other hand, the irradiation period was reduced to 15 min to minimize nonselective phototoxic effects. Indeed, the latter is clearly demonstrated by the data in Fig. 4c, which was again measured by incubating the cells with polybenzoxazine nanoparticles for 24 h before photoexcitation and analyzing cell viability at 0 h and 48 h after photoexcitation. No statistically meaningful differences in cell survival were observed in this case for the irradiated polybenzoxazine-free control samples relative to those kept in the dark. On the contrary, large phototoxicity effects were registered when loaded with **PBz1** nanostructures, which led to a noteworthy decrement in cell viability upon illumination (<50 % at 48 h post-irradiation, Fig. 4c). Though we cannot exclude that photoinduced reactive oxygen species (ROS) contributed to cell death in these experiments, we ascribe the phototoxicity effects observed principally to PTT because: (a) photothermal heating was indeed measured for **PBz1_NP1** and **PBz1_NP2** in cell culture medium at similar concentrations (see Fig. 3b); and (b) polyphenols such as polybenzoxazines as well as other benzoxazine derivatives are known to exhibit antioxidant properties and, therefore, contribute to ROS scavenging [31,42,43].

Despite its lower concentration, the best of these PTT effects were obtained for **PBz1_NP2**, whose red light-induced photothermal heating promoted the death of about 70 % of the initial SKBR-3 cells. This is a remarkable result when compared to previous reports on the photothermal treatment of SKBR-3 cells in vitro (Table S1) [44–54]. Although it does not match the best figures reported in the literature (~100 % cell death [51,52]), **PBz1_NP2** provides higher phototoxicity at lower concentration and/or irradiation dose than many of the PTT agents so far described [44–46,48–49,54]. Therefore, in combination with their simple preparation and low cytotoxicity in the dark, these results make **PBz1_NP2** very promising materials for photothermal therapy.

Importantly, the high PTT activity of **PBz1** nanoparticles was preserved when shorter incubation times were applied. For instance, after treatment of SKBR-3 cells with **PBz1_NP1** (0.86 mg mL^{-1}) and **PBz1_NP2** (0.43 mg mL^{-1}) for only 4 h followed by exhaustive rinsing, we still observed cell viability to decrease well below 60 % post-irradiation (Fig. S10). This result suggested that efficient internalization of **PBz1_NP1** and **PBz1_NP2** occurs within the cells. We further investigated this aspect by taking advantage of the orange emission detected for **PBz1** nanostructures in cell cultures under the confocal microscope, which spectrally resembled the fluorescence measured for the same nanomaterials in aqueous suspension ($\lambda_{em,\ max} \sim 600$ nm; Fig. S11). As a result, we could investigate the internalization of **PBz1_NP1** and **PBz1_NP2** in SKBR-3 cells by confocal microscopy, for which we also stained their plasma membrane with the green-emitting dye WGA-488. Although we observed the presence of **PBz1** nanoparticles outside the cells, polybenzoxazine orange fluorescence could also be measured in their interior, thus suggesting cell internalization for both 4 h and 24 h incubation protocols (Fig. 5 and Fig. S12). This was unambiguously proven by collecting optical sections of the fluorescence images in the axial direction of the samples, which confirmed that some of the orange-emitting **PBz1** structures lay confined within the interior of SKBR-3 cells (Fig. 5 and Fig. S12). Because of the local nature of photothermal effects, we ascribe the phototoxic effects measured to these internalized nanostructures as well as those adhered to the cell membrane. In addition, it must be noted that the highest PTT efficiencies were observed for the low **PBz1_NP2** concentration used, where a

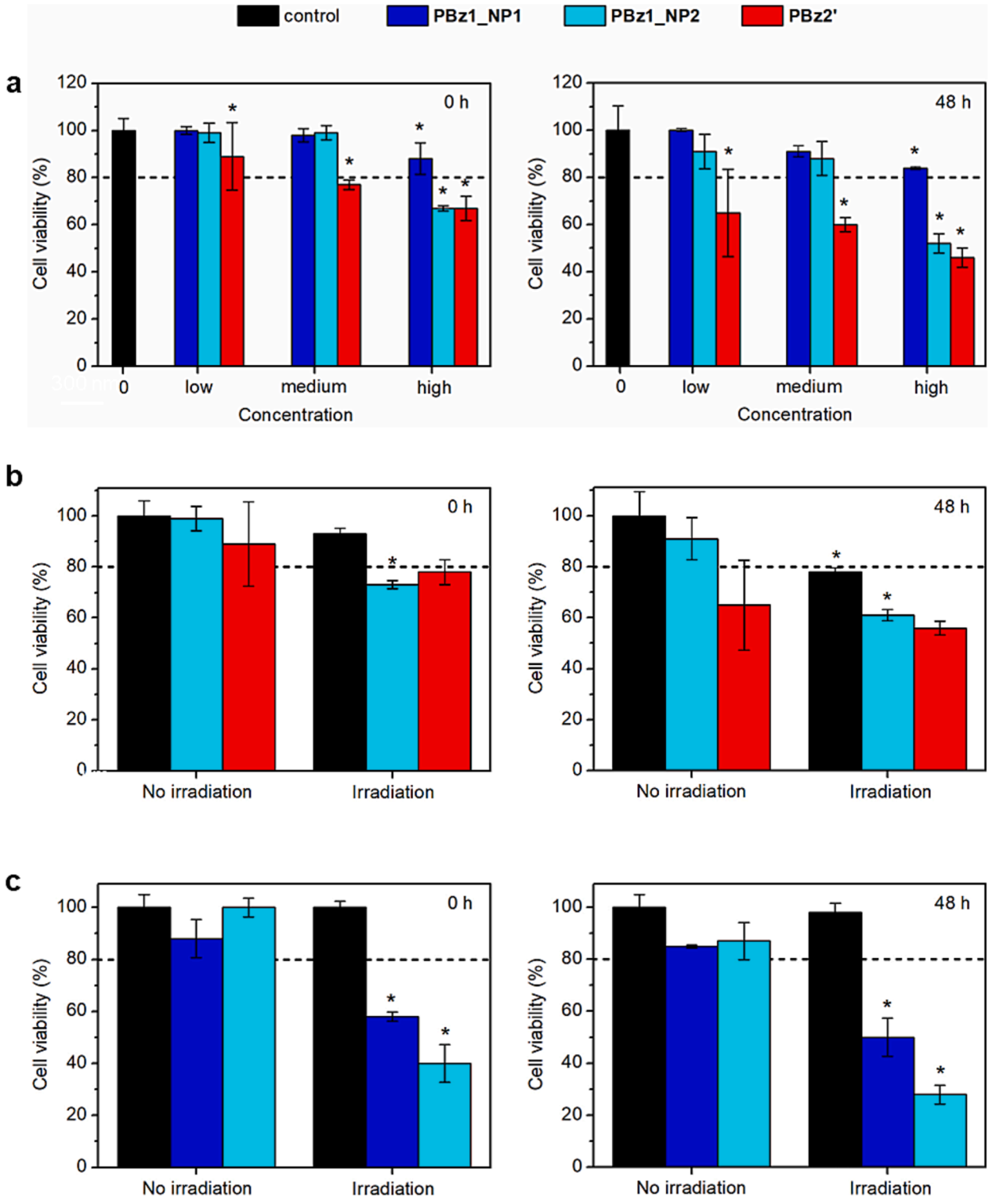

Fig. 4. (a) Cell viability analysis after incubation for 24 h with different concentrations of **PBz1_NP1**, **PBz1_NP2** and **PBz2′** in the dark (control = 0 mg mL^{-1}; low = 0.22 mg mL^{-1} for **PBz1_NP1** and **PBz1_NP2**, and 0.23 mg mL^{-1} for **PBz2′**; medium = 0.43 mg mL^{-1} for **PBz1_NP1** and **PBz1_NP2**, and 0.46 mg mL^{-1} for **PBz2′**; high = 0.86 mg mL^{-1} for **PBz1_NP1** and **PBz1_NP2**, and 0.91 mg mL^{-1} for **PBz2′**). Measurements were taken at two distinct post-incubation times: 0 h (left) and 48 h (right). Asterisks indicate statistically significant differences in cell viability between the control and the incubated samples at each time-point. (b) Cell viability analysis after incubation for 24 h with **PBz1_NP2** (0.22 mg mL^{-1}) and **PBz2′** (0.23 mg mL^{-1}) and subsequent irradiation for 30 min at λ_{exc} = 620 – 630 nm (power density = 55 mW cm^{-2}). Measurements were taken at two distinct post-irradiation times: 0 h and 48 h. (c) Cell viability analysis after incubation for 24 h with **PBz1_NP1** (0.86 mg mL^{-1}) and **PBz1_NP2** (0.43 mg mL^{-1}) and subsequent irradiation for 15 min at λ_{exc} = 620 – 630 nm (power density = 55 mW cm^{-2}). Measurements were taken at two distinct post-irradiation times: 0 h and 48 h. In (b-c) asterisks indicate statistically significant differences in the cell viability between the same not irradiated and irradiated treatment at each time-point. Experiments were done in triplicates.

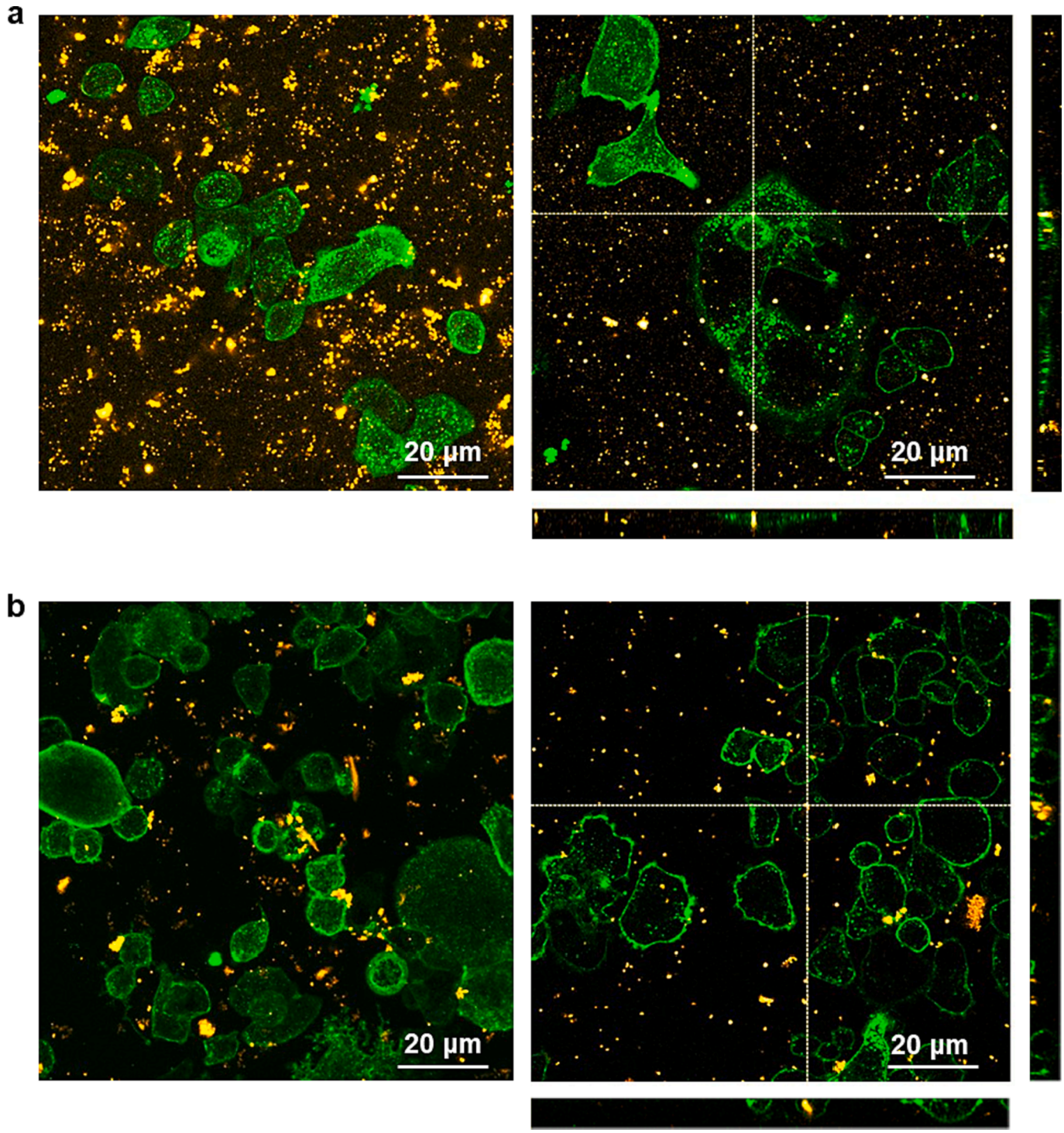

Fig. 5. Confocal fluorescence emission images ($\lambda_{exc} = 405$ nm, $\lambda_{em} = 569 – 611$ nm) of SKBR-3 cells incubated with (a) **PBz1_NP1** (0.86 mg mL^{-1}) and (b) **PBz1_NP2** (0.43 mg mL^{-1}) for 4 h and subsequently rinsed. In both cases the plasma membrane of cells was stained by previous treatment with green-emitting dye WGA-488, whose fluorescence was detected simultaneously in a different channel ($\lambda_{exc} = 488$ nm, $\lambda_{em} = 500 – 550$ nm). The images in the right show additional Z-stacks for two orthogonal cross-sections (indicated by white dashed lines). (For interpretation of the references to colour in this figure legend, the reader is referred to the web version of this article.)

reduced number of residual, non-internalized nanoparticles were found in the cell culture medium (Fig. 5b). Consequently, we expect the external nanostructures to have a minimal contribution to photothermally-induced cell death.

3. Conclusions

In this work we reported the application of polybenzoxazines, a well-known class of phenolic resins, to photothermal therapy. For this, two different types of strategies were explored: the use of water-soluble polybenzoxazines as molecular photothermal agents and of nanoparticles made from hydrophobic polybenzoxazines as nanostructurated

photothermal materials. Interestingly, the latter could not only be prepared a priori employing well-known emulsion techniques, but also in situ by nanoprecipitation when adding the polymers to cell culture medium. All the resulting polybenzoxazine compounds and materials exhibited a broad absorption tail in the visible spectrum and generated photothermal heating upon irradiation with visible light. When tested in vitro on human breast cancer cells, water-soluble polybenzoxazines showed significant cytotoxicity in the dark, which only moderately increased upon irradiation. By contrast, polybenzoxazine nanoparticles were found to cause cancer cells' death selectively and efficiently when illuminated with high-penetrating red light. Thanks to their fluorescent properties that allowed microscopy colocalization experiments, this phototoxic behavior could be attributed to the internalization of the nanoparticles within the cells and the subsequent photothermal effects induced under irradiation. Together with their low cost, simple structure and facile preparation, these features make polybenzoxazine nanoparticles very promising materials for photothermal therapy.

4. Materials and methods

4.1. Materials for monomer, polymer and nanostructure synthesis

Reagents (aniline, paraformaldehyde, 4-methoxyphenol, 4-hydroxybenzoic acid) and solvents (toluene, 1,4-dioxane, dichloromethane, water, $CDCl_3$, acetone-d_6 and DMSO-d_6) for the synthesis of **Bz1**, **Bz2**, **PBz1**, **PBz2** and **PBz2′** as well as the nanoparticles of **PBz1** were purchased and used without further purification. Thin layer chromatography (TLC) was performed using Macherey-Nagel aluminum backed plates of silica gel (60 Å pore size) with fluorescent indicator UV254 (Alugram®, 0.2 mm thickness). Flash column chromatography was performed using silica gel (230–400 mesh).

4.2. Synthesis of polymers PBz1, PBz2 and PBz2′

Benzoxazine monomers **Bz1** [36] and **Bz2** [37] were synthesized as previously described (Scheme S1). **Bz1** and **Bz2** were then introduced in a glass vial and placed in a sand bath at 180 and 200 °C, respectively. After 2 h, polybenzoxazines **PBz1** and **PBz2** were afforded. Both samples were crushed into powder to facilitate their solubility and dispersion. To prepare **PBz2′**, polybenzoxazine **PBz2** was placed in an equimolar NaOH aqueous solution and stirred for 24 h at room temperature. The suspension turned from transparent to yellow over time and we observed dissolution of most of the initial solid. The final mixture was filtered in order to eliminate the unreacted polymer and the solvent was removed at reduced pressure, obtaining polybenzoxazine salt **PBz2′** as a yellow solid.

4.3. Nanostructuration of PBz1

For the preparation of **PBz1** nanoparticles via emulsion in water (**PBz1_NP1**), the following procedure was carried out. First, polybenzoxazine **PBz1** (86.2 mg) was completely solved in 1 mL of dichloromethane and placed in a glass vial (Ø = 70 mm, h = 22 mm) with 20 mL of Milli-Q water. The mixture was sonicated using an ultrasonic homogenizer operating at 70 % amplitude (Branson 450 D Sonifier, 400 W–20 kHz, equipped with disruptor horn and 13 mm flat tip) during 5 min, which afforded a homogeneous orange emulsion. Dichloromethane was then removed under vacuum to obtain a stock aqueous colloidal suspension of **PBz1_NP1** (4.3 mg mL^{-1}). This sample was further diluted in cell culture medium (see section 4.4) to prepare 0.86 mg mL^{-1}, 0.43 mg mL^{-1} and 0.22 mg mL^{-1} colloidal suspensions of **PBz1_NP1**.

For the direct preparation of **PBz1** nanoparticles via nanoprecipitation in cell culture medium (**PBz1_NP2**), we first completely dissolved polybenzoxazine **PBz1** (86.2 mg) in 1 mL of DMSO. Then, 40 μL of this solution were added dropwise to 360 μL of cell culture medium (see Section 4.4) under vigorous stirring (700 rpm). As a result, an ochre-colored colloidal suspension of **PBz1_NP2** (8.6 mg mL^{-1}) was obtained. This sample was further diluted in more cell culture medium to prepare 0.86 mg mL^{-1}, 0.43 mg mL^{-1} and 0.22 mg mL^{-1} colloidal suspensions of **PBz1_NP2**. Because of the rather poor colloidal stability of these samples, all of them were freshly prepared before each biological experiment.

4.4. Cell culture assays

SKBR-3 cells, a tumorigenic human mammary epithelial cell line (ATCC, USA), were used for biological experiments. Unless stated otherwise, cells were cultured in McCoy's 5A modified medium (Gibco, UK) supplemented with 10 % fetal bovine serum (Gibco) in a 37 °C humidified incubator and set to 5 % CO_2 (standard culture conditions). For dark toxicity evaluation and photothermal therapy experiments, cells were seeded in 4- or 24-well plates at a density of 3.50×10^4 cells per well. For confocal microscopy experiments, cells were seeded in 35 mm confocal dishes provided with glass coverslip bottom (μ-Dish 35 mm, high Grid-500 Glass Bottom, Ibidi, DE) at a density of 1.75×10^5 cells per well. All experiments were performed 24 h after seeding. Incubation of cells with polybenzoxazine nanoparticles **PBz1_NP1** and **PBz1_NP2** was done using the 0.86 mg mL^{-1}, 0.43 mg mL^{-1} and 0.22 mg mL^{-1} colloidal suspensions prepared directly in cell culture medium (see section 4.3). For water-soluble polymer **PBz2′** incubation, polymer was first dissolved in filtered Milli-Q water to a final concentration of 96.4 mg mL^{-1}. This stock solution was then diluted in cell culture medium obtaining a final compound concentration of 0.91 mg mL^{-1}, 0.46 mg mL^{-1} and 0.23 mg mL^{-1}.

Polymer toxicity in absence of irradiation was determined by assessing cell viability by the AlamarBlue™ assay (ThermoFisher Scientific) at two different time-points (0 h and 48 h post-incubation). 24 h after cell seeding, cells were incubated for 24 h with different concentrations of **PBz1** nanoparticles (0 (control), 0.86 mg mL^{-1}, 0.43 mg mL^{-1} and 0.22 mg mL^{-1}) and **PBz2′** (0 (control), 0.91 mg mL^{-1}, 0.46 mg mL^{-1} and 0.23 mg mL^{-1}). Then, cell medium was removed, and cells were washed four times with Hank's Balanced Salt Solution (HBSS, BioWest, MO, USA) to remove any remaining product. Finally, fresh medium was added. At that point, viability was immediately assessed (cell viability 0 h) or cultures were kept in standard culture conditions for 48 h more before cell viability evaluation (cell viability 48 h). Three independent experiments were conducted for each condition.

The same protocol as described in the previous paragraph was followed for photothermal treatments, though incubation of SKBR-3 cells with **PBz1** nanoparticles and **PBz2′** took place for 4 or 24 h. Then, cells were either kept in dark conditions or irradiated for 15–30 min in the wavelength range of 620 – 630 nm. Cell culture viability was measured right after irradiation (cell viability 0 h) by using the AlamarBlue™ assay or cultures were kept in standard culture conditions for 48 h more before cell viability evaluation (cell viability 48 h). Three independent experiments were performed for each condition.

Cell viability was determined by the AlamarBlue™ cell viability reagent. After polymer incubation and, if needed, irradiation, medium was removed and cells were washed four times with HBSS, before adding fresh medium with 10 % AlamarBlue™. Cells were incubated for 4 h in standard conditions in the dark. Finally, supernatant was collected and 200 μL of the solution were transferred to a black bottom Greiner CELLSTAR® 96-well plate (Sigma-Aldrich®) to measure its fluorescence at 590 nm, after excitation at $\lambda_{exc} = 560$ nm. Three independent experiments were performed for each condition.

For measuring **PBz1** nanoparticles emission spectrum, cells were seeded on 35 mm confocal dishes, provided with glass coverslip bottom at a density of 1.75×10^5 cells/dish and incubated in standard conditions in the dark. After 24 h, a 0.43 mg mL^{-1} colloidal suspension of **PBz1_NP2** was added, and the cell culture was incubated for another 24 h in the same conditions. Then, a Lambda Scan experiment was

performed in a confocal fluorescence microscope to determine the emission spectrum of the nanoparticles, for which the excitation wavelength was set up at $\lambda_{exc} = 405$ nm. For post-treated cultures, cells were washed four times with HBSS and the same procedure was performed, before the new image acquisition.

To investigate **PBz1_NP1** and **PBz1_NP2** internalization, cells were seeded on a 35 mm confocal dish provided with glass coverslip bottom (1.75×10^5 cells). After 24 h, a 0.86 mg mL^{-1} colloidal suspension of **PBz1_NP1** or a 0.43 mg mL^{-1} colloidal suspension of **PBz1_NP2** were added to the culture. After incubating for 4 h and 24 h in standard conditions in the dark, respectively, cells were washed four times with HBSS to remove the non-internalized product and incubated with WGA-Alexa Fluor 488 (5 μL) for 15 min to stain the plasma membrane. Images of the resulting samples were acquired by sequential excitation of WGA-Alexa Fluor 488 at $\lambda_{exc} = 488$ nm and **PBz1** nanostructures at $\lambda_{exc} = 405$ nm, whose emission was separately detected in different spectral ranges: $\lambda_{em} = 569–611$ nm for **PBz1_NP1** and **PBz1_NP2** emission, and $\lambda_{em} = 500–550$ nm for WGA-Alexa Fluor 488.

4.5. Characterization methods

^{1}H NMR spectra were recorded on a Bruker DPX360 (360 MHz) spectrometer in $CDCl_3$, acetone-d_6 and DMSO-d_6. The δ-scale was normalized relative to the residual solvent signal ($CDCl_3$: 7.26 ppm, acetone-d_6: 2.05 ppm and DMSO-d_6: 2.49 ppm). Infrared spectra were measured on a Bruker Tensor 27 Golden Gate spectrometer in attenuated total reflectance mode (IR-ATR). The UV–vis absorption spectra of liquid samples, solutions and colloidal suspensions were measured with an Agilent 8453 UV–visible spectrophotometer using Hellma Analytics glass cuvettes (1-cm light path). Fluorescence spectra were recorded by means of a custom-made spectrofluorometer using a cw diode laser ($\lambda_{exc} = 445$ nm) as the excitation source. Emitted photons were detected using an Andor ICCD camera coupled to a spectrograph. All the emission spectra registered were corrected by the wavelength dependence of the spectral response of the detection system. Molecular weight distributions were determined by gel permeation chromatography (GPC) using an Agilent Technologies 1260 Infinity chromatograph and THF as a solvent. The instrument was equipped with three gel columns: PLgel 5 μm Guard/50 × 7.5 mm, PLgel 5 μm 10000 Å MW 4 K − 400 K, and PL Mixed gel C 5 μm MW 200——3 M. Calibration was made by using PMMA standards. Differential scanning calorimetry (DSC) experiments were conducted with a TA Instruments Q20 calorimeter using Tzero™ pans and lids calibrated with indium ($T_m = 429.75$ K, $\Delta H_m = 3267$ kJ/mol). For all the samples, we used a heating rate of 10 °C/min and a N_2 flow of 50 mL/min. The gel content of **PBz1** and **PBz2** was determined as previously reported by us.[55] About 1.0 g of the polymer material of interest were subjected to a 24 h Soxhlet extraction using acetone as a solvent. This led to dissolution of linear polymer chains, leaving behind the insoluble cross-linked 3D network. Therefore, comparison of the final insoluble material left in the cellulose cartridge used in the extraction (m_{gel}) with the initial polymer mass (m_0) allowed us the calculation of the gel content using equation (1):

$$Gel\ content(\%) = \frac{m_{gel}}{m_0} \cdot 100 \quad (1)$$

Scanning electron microcopy (SEM) images of the polymer nanoparticles were taken using a Zeiss Merlin scanning electron microscope and analyzed by means of the ImageJ software. All the samples were metalized with a layer of about 5 nm of Pt prior to SEM imaging. Dynamic light scattering (DLS) measurements to characterize their nanoparticle diameters and ζ-potentials were measured in a Malvern Zetasizer Nano ZS apparatus. Cell culture irradiation experiments were performed using a GenIUL photoactivation universal light device ($\lambda_{exc} = 620 – 630$ nm; power density = 55 mW/cm^2; energy dose: 33 J/cm^2). Fluorescence confocal images were acquired in a Leica TCS-SP5 AOBS spectral Confocal Laser Scanning Microscope (Leica Microsystems) using a Plan-Apochromatic 63X objective lens ($\lambda_{exc} = 405$ nm). Further image analysis was performed with Fiji software. The fluorescence spectrum of the internalized polymers was registered using the same microscope operating in Lamba Scan mode. Cell statistical analyses were performed by using GraphPad Prism software (6.01 version, Windows). Results were analyzed through a two-way ANOVA factorial analysis. Minimal significance level set at $P \leq 0.05$. Significance is represented in the figures using an asterisk. Values with an asterisk are significantly different from their control ($P = 0.05$).

Author Contributions

K.R.-M. and O.C. conducted the synthetic, characterization and biological experiments, while J.H., C.N. and R.M.S. devised the project and supervised the experimental work. The manuscript was written through contributions of all authors. All authors have given approval to the final version of the manuscript.

Declaration of Competing Interest

The authors declare that they have no known competing financial interests or personal relationships that could have appeared to influence the work reported in this paper.

Data availability

Data available in the CORA.RDR, Research Data Repository (https://dataverse.csuc.cat/): https://doi.org/10.34810/data906 (accessed on 03 November 2023).

Acknowledgements

This work was supported by grants PID2019-106171RB-I00 and PID2020-116844RB-C21 (funded by MCIN/AEI/10.13039/501100011033 and ERDF–"A way of making Europe"), and 2021 SGR 00064 and 2021 SGR 00122 (funded by AGAUR, Generalitat de Catalunya). K.R.-M. and O.C. thanks Universitat Autònoma de Barcelona for their predoctoral fellowship. The authors would like to thank the staff from the Servei de Microscòpia of Universitat Autònoma de Barcelona.

Appendix A. Supplementary data

Supplementary data to this article can be found online at https://doi.org/10.1016/j.eurpolymj.2023.112531.

References

[1] L. Zou, H. Wang, B. He, L. Zeng, T. Tan, H. Cao, X. He, Z. Zhang, S. Guo, Y. Li, Current approaches of photothermal therapy in treating dancer metastasis with nanotherapeutics, Theranostics 6 (2016) 762–772, https://doi.org/10.7150/thno.14988.

[2] X. Li, J.F. Lovell, J. Yoon, X. Chen, Clinical development and potential of photothermal and photodynamic therapies for cancer, Nat. Rev. Clin. Oncol. 17 (2020) 657–674, https://doi.org/10.1038/s41571-020-0410-2.

[3] G. Cao, X. Sun, G. Liang, Nanoagent-promoted mild-temperature photothermal therapy for cancer treatment, Adv. Funct. Mater. 31 (2021) 2100738, https://doi.org/10.1002/adfm.202100738.

[4] L. Cheng, C. Wang, L. Feng, K. Yang, Z. Liu, Functional nanomaterials for phototherapies of cancer, Chem. Rev. 114 (2014) 10869–10939, https://doi.org/10.1021/cr400532z.

[5] S. Gai, G. Yang, P. Yang, F. He, J. Lin, D. Jin, B. Xing, Recent advances in functional nanomaterials for light–triggered cancer therapy, Nano Today 19 (2018) 146–187, https://doi.org/10.1016/j.nantod.2018.02.010.

[6] W. Bian, Y. Wang, Z. Pan, N. Chen, X. Li, W.-L. Wong, X. Liu, Y. He, K. Zhang, Y.-J. Lu, Review of functionalized nanomaterials for photothermal therapy of cancers, ACS Appl. Nano Mater. 4 (2021) 11353–11385, https://doi.org/10.1021/acsanm.1c01903.

[7] Y. Yang, X. Fan, L. Li, Y. Yang, A. Nuernisha, D. Xue, C. He, J. Qian, Q. Hu, H. Chen, J. Liu, W. Huang, Semiconducting polymer nanoparticles as theranostic system for near-infrared-II fluorescence imaging and photothermal therapy under safe laser fluence, ACS Nano 14 (2020) 2509–2521, https://doi.org/10.1021/acsnano.0c00043.

[8] T.T.V. Phan, V.T. Nguyen, S.-H. Ahn, J. Oh, Chitosan-mediated facile green synthesis of size-controllable gold nanostars for effective photothermal therapy and photoacoustic imaging, Eur. Polym. J. 118 (2019) 492–501, https://doi.org/10.1016/j.eurpolymj.2019.06.023.

[9] W. Fan, B. Yung, P. Huang, X. Chen, Nanotechnology for multimodal synergistic cancer therapy, Chem. Rev. 117 (2017) 13566–13638, https://doi.org/10.1021/acs.chemrev.7b00258.

[10] Y. Sheng, C. Cao, Z. Liang, Z.-Z. Yin, J. Gao, W. Cai, Y. Kong, Construction of a dual-drug delivery system based on oxidized alginate and carboxymethyl chitosan for chemo-photothermal synergistic therapy of osteosarcoma, Eur. Polym. J. 174 (2022), 111331, https://doi.org/10.1016/j.eurpolymj.2022.111331.

[11] H.-C. Huang, S. Barua, G. Sharma, S.K. Dey, K. Rege, Inorganic nanoparticles for cancer imaging and therapy, J. Control. Release 155 (2011) 344–357, https://doi.org/10.1016/j.jconrel.2011.06.004.

[12] E. Boisselier, D. Astruc, Gold nanoparticles in nanomedicine: preparations, imaging, diagnostics, therapies and toxicity, Chem. Soc. Rev. 38 (2009) 1759–1782, https://doi.org/10.1039/B806051G.

[13] E.C. Dreaden, M.A. Mackey, X. Huang, B. Kang, M.A. El-Sayed, Beating cancer in multiple ways using nanogold, Chem. Soc. Rev. 40 (2011) 3391–3404, https://doi.org/10.1039/C0CS00180E.

[14] G. Hong, S. Diao, A.L. Antaris, H. Dai, Carbon nanomaterials for biological imaging and nanomedicinal therapy, Chem. Rev. 115 (2015) 10816–10906, https://doi.org/10.1021/acs.chemrev.5b00008.

[15] V.P. Jain, S. Chaudhary, D. Sharma, N. Dabas, R.S.K. Lalji, B.K. Singh, G. Jaiswar, Advanced functionalized nanographene oxide as a biomedical agent for drug delivery and anti-cancerous therapy: A review, Eur. Polym. J. 142 (2021), 110124, https://doi.org/10.1016/j.eurpolymj.2020.110124.

[16] X. Huang, W. Zhang, G. Guan, G. Song, R. Zou, J. Hu, Design and functionalization of the NIR-responsive photothermal semiconductor nanomaterials for cancer theranostics, Acc. Chem. Res. 50 (2017) 2529–2538, https://doi.org/10.1021/acs.accounts.7b00294.

[17] X. Song, Q. Chen, Z. Liu, Recent advances in the development of organic photothermal nano-agents, Nano Res. 8 (2015) 340–354, https://doi.org/10.1007/s12274-014-0620-y.

[18] L. Xu, L. Cheng, C. Wang, R. Peng, Z. Liu, Conjugated polymers for photothermal therapy of cancer, Polym. Chem. 5 (2014) 1573–1580, https://doi.org/10.1039/C3PY01196H.

[19] J. Li, J. Rao, K. Pu, Recent progress on semiconducting polymer nanoparticles for molecular imaging and cancer phototherapy, Biomaterials 155 (2018) 217–235, https://doi.org/10.1016/j.biomaterials.2017.11.025.

[20] H.S. Jung, P. Verwilst, A. Sharma, J. Shin, J.L. Sessler, J.S. Kim, Organic molecule-based photothermal agents: an expanding photothermal therapy universe, Chem. Soc. Rev. 47 (2018) 2280–2297, https://doi.org/10.1039/C7CS00522A.

[21] Y. Cai, W. Si, W. Huang, P. Chen, J. Shao, X. Dong, Organic dye based nanoparticles for cancer phototheranostics, Small 14 (2018) 1704247, https://doi.org/10.1002/smll.201704247.

[22] H. Ishida, T. Agag, Handbook of benzoxazine resins, first ed., Elsevier, 2011.

[23] H. Ishida, P. Froimowicz, Advanced and emerging polybenzoxazine science and technology, first ed., Elsevier, 2017.

[24] I. Machado, C. Shaer, K. Hurdle, V. Calado, H. Ishida, Towards the development of green flame retardancy by polybenzoxazines, Prog. Polym. Sci. 121 (2021), 101435, https://doi.org/10.1016/j.progpolymsci.2021.101435.

[25] Y. Liu, H. Ishida, Natural-sourced benzoxazine resins, homopolymers, blends and composites: A review of their synthesis, manufacturing and applications, Prog. Polym. Sci. 99 (2019), 101168, https://doi.org/10.1016/j.progpolymsci.2019.101168.

[26] V. Vatanpour, B. Kiskan, B. Zeytuncu, I. Kayuncu, Polybenzoxazines in fabrication of separation membranes: A review, Sep. Purif. Technol. 278 (2021), 119562, https://doi.org/10.1016/j.seppur.2021.119562.

[27] B. Kiskan, N.N. Ghosh, Y. Yagci, Polybenzoxazine-based composites as high-performance materials, Polym. Int. 60 (2011) 167–177, https://doi.org/10.1002/pi.2961.

[28] X. Fan, S. Li, C. Wang, Y. Deng, C. Zhang, Z. Wang, Research on fluoropyridine-based benzoxazine with high thermal stability and excellent flame retardancy for its application in coatings, Eur. Polym. J. 187 (2023), 111884, https://doi.org/10.1016/j.eurpolymj.2023.111884.

[29] D.A. Rubenstein, H. Lu, S.S. Mahadik, N. Leventis, W. Yin, Characterization of the physical properties and biocompatibility of polybenzoxazine-based aerogels for use as a novel hard-tissue scaffold, J. Biomater. Sci. 23 (2012) 1171–1184, https://doi.org/10.1163/092050611x576954.

[30] L. Lotfi, J. Javadpour, M.R. Naimi-Jamal, Biological and nano-indentation properties of polybenzoxazine-based composites reinforced with zirconia particles as a novel biomaterial, Biomed. Mater. Eng. 29 (2018) 369–387, https://doi.org/10.3233/bme-181731.

[31] N. Yadav, M. Monisha, R. Niranjan, A. Dubey, S. Patil, R. Priyadarshini, B. Lochab, Antibacterial performance of fully biobased chitosan-grafted-polybenzoxazine films: Elaboration and properties of released material, Carbohydr. Polym. 254 (2021), 117296, https://doi.org/10.1016/j.carbpol.2020.117296.

[32] Q. Ma, X. Liu, H. Wang, Q. Zhuang, J. Qian, Construction of novel benzoxazine-linked covalent organic framework with antimicrobial activity via postsynthetic cyclization, Mater. Today Chem. 23 (2022), 100707, https://doi.org/10.1016/j.mtchem.2021.100707.

[33] S. Sahu, R. Niranjan, R. Priyadarshini, B. Lochab, Benzoxazine-grafted-chitosan biopolymer films with inherent disulfide linkage: Antimicrobial properties, Chemosphere 328 (2023), 138587.

[34] X. Yuan, X. Su, Y. Wang, L. Liu, R. Li, C. Wang, Benzoxazine monomers with antibacterial property and polybenzoxazines for preventing adhesion to bacteria, ACS Appl. Polym. Mater. 5 (2023) 5650–5651, https://doi.org/10.1021/acsapm.3c00943.

[35] K. Reyes-Mateo, J. Marquet, J. Hernando, R.M. Sebastián, Photothermal polymerization of benzoxazines, Polym. Chem. 13 (2022) 5256–5264, https://doi.org/10.1039/D2PY00635A.

[36] J. Salabert, R.M. Sebastián, J. Marquet, Photochemical polymerization of N-phenyl mono-1,3-benzoxazines in aqueous media, Macromolecules 51 (2018) 3672–3679, https://doi.org/10.1021/acs.macromol.8b00171.

[37] R. Andreu, M. Espinosa, M. Galia, V. Cádiz, J.C. Ronda, J.A. Reina, Synthesis of novel benzoxazines containing glycidyl groups: A study of the crosslinking behavior, J. Polym. Sci. A Polym. Chem. 44 (2006) 1529–1540, https://doi.org/10.1002/pola.21255.

[38] N. Anton, J.-P. Benoit, P. Saulnier, Design and production of nanoparticles formulated from nano-emulsion templates—A review, J. Control. Release 128 (2008) 185–199, https://doi.org/10.1016/j.jconrel.2008.02.007.

[39] C.I. Crucho, M.T. Barros, Polymeric nanoparticles: A study on the preparation variables and characterization methods, Mat. Sci. Eng. C 80 (2017) 771–784, https://doi.org/10.1016/j.msec.2017.06.004.

[40] J.P. Rao, K.E. Geckeler, Polymer nanoparticles: Preparation techniques and size-control parameters, Prog. Polym. Sci. 36 (2011) 887–913, https://doi.org/10.1016/j.progpolymsci.2011.01.001.

[41] X. Yan, J. Bernard, F. Ganachaud, Nanoprecipitation as a simple and straightforward process to create complex polymeric colloidal morphologies, Adv. Colloid Interface Sci. 294 (2021), 102474, https://doi.org/10.1016/j.cis.2021.102474.

[42] T. Kundu, B. Bhattacharjee, S. Hazra, A.K. Ghosh, D. Bandyopadhyay, A. Pramanik, Synthesis and biological assessment of pyrrolobenzoxazine scaffold as a potent antioxidant, J. Med. Chem. 62 (2019) 6315–6329, https://doi.org/10.1021/acs.jmedchem.9b00717.

[43] S.R. Sangani, Y. Yao, R.C. Dabhi, M. Kawad, J. Parmar, M. Afzal, A. Alarifi, C. B. Sangani, R.K. Ameta, Y.-T. Duan, BSA/HAS interaction and antioxidant evaluation of newly synthesized benzoxazine derivatives: Spectrophotometric and molecular docking studies, J. Mol. Liq. 389 (2023), 122917, https://doi.org/10.1016/j.molliq.2023.122917.

[44] M. Hashemkhani, E. Celikbas, M. Khan, A. Sennaroglu, H.Y. Acar, ALA/Ag2S/MnO2 hybrid nanoparticles for near-infrared image-guided long-wavelength phototherapy of breast cancer, ACS Biomater Sci. Eng. 9 (2023) 4126–4137, https://doi.org/10.1021/acsbiomaterials.3c00105.

[45] F. Khakbaz, M. Mirzaei, M. Mahani, Lecithin sensitized thermo-sensitive niosome using NIR-carbon dots for breast cancer combined chemo-photothermal therapy, J. Photochem. Photobiol. A Chem. 434 (2023), 114326, https://doi.org/10.1016/j.jphotochem.2022.114236.

[46] B. Dorjsuren, B. Chaurasiya, Z. Ye1, Y. Liu, W. Li, C. Wang, D. Shi, C.E. Evans, T. J. Webster, Y. Shen, Cetuximab-coated thermo-sensitive liposomes loaded with magnetic nanoparticles and doxorubicin for targeted EGFR-expressing breast cancer combined therapy, Int. J. Nanomed. 15 (2020) 8201–8215, https://doi.org/10.2147/IJN.S261671.

[47] Y. Zhang, C.-F. Wan, J. Du, Q. Dong, Y.-Y. Wang, H. Yang, F.-H. Li, The in vitro study of Her-2 targeted gold nanoshell liquid fluorocarbon poly lactic-co-glycolic acid ultrasound microcapsule for ultrasound imaging and breast tumor photothermal therapy, J. Biomater. Sci. Polym. Ed. 29 (2018) 57–73, https://doi.org/10.1080/09205063.2017.1399003.

[48] L. Deng, X. Cai, D. Sheng, Y. Yang, E.M. Strohm, Z. Wang, H. Ran, D. Wang, Y. Zheng, P. Li, T. Shang, Y. Ling, F. Wang, Y. Sun, A laser-activated biocompatible theranostic nanoagent for targeted multimodal imaging and photothermal therapy, Theranostics 7 (2017) 4410–4423, https://doi.org/10.7150/thno.21283.

[49] X. Kang, X. Guo, X. Niu, W. An, S. Li, Z. Liu, Y. Yang, N. Wang, Q. Jiang, C. Yan, H. Wang, Q. Zhang, Photothermal therapeutic application of gold nanorods-porphyrin-trastuzumab complexes in HER2-positive breast cancer, Sci. Rep. 7 (2017) 42069, https://doi.org/10.1038/srep42069.

[50] G. Feng, Y. Fang, J. Liu, J. Geng, D. Ding, B. Liu, Multifunctional conjugated polymer nanoparticles for image-guided photodynamic and photothermal therapy, Small 13 (2017) 1602807, https://doi.org/10.1002/smll.201602807.

[51] N. Gandra, C. Portz, S.Z. Nergiz, A. Fales, T. Vo-Dinh, S. Singamaneni, Inherently stealthy and highly tumor-selective gold nanoraspberries for photothermal cancer therapy, Sci. Rep. 5 (2015) 10311, https://doi.org/10.1038/srep10311.

[52] S.Z. Nergiz, N. Gandra, S. Tadepalli, S. Singamaneni, Multifunctional hybrid nanopatches of graphene oxide and gold nanostars for ultraefficient photothermal cancer therapy, ACS Appl. Mater. Interfaces 6 (2014) 16395–16402, https://doi.org/10.1021/am504795d.

[53] Y.-C. Chuang, C.-J. Lin, S.-F. Lo, J.-L. Wang, S.-C. Tzou, S.-S. Yuan, Y.-M. Wang, Dual functional AuNRs@MnMEIOs nanoclusters for magneticresonance imaging and photothermal therapy, Biomater. 35 (2014) 4678–4687, https://doi.org/10.1016/j.biomaterials.2014.02.026.

[54] L. Au, D. Zheng, F. Zhou, Z.Y. Li, X. Li, Y. Xia, A quantitative study on the photothermal effect of immuno gold nanocages targeted to breast cancer cells, ACS Nano 2 (2008) 1645–1652, https://doi.org/10.1021/nn800370j.

[55] A. Martos, M. Soto, H. Schäfer, K. Koschek, J. Marquet, R.M. Sebastián, Highly crosslinked polybenzoxazines from monobenzoxazines: The effect of meta-substitution in the phenol ring, Polymers 12 (2020) 254, https://doi.org/10.3390/polym12020254.